International Journal of Sustainable Energy

ISSN: 1478-6451 (Print) 1478-646X (Online) Journal homepage: http://www.tandfonline.com/loi/gsol20

A framework for determining improved placement of current energy converters subject to environmental constraints

Kurt Nelson, Scott C. James, Jesse D. Roberts & Craig Jones

To cite this article: Kurt Nelson, Scott C. James, Jesse D. Roberts & Craig Jones (2018) A framework for determining improved placement of current energy converters subject to environmental constraints, International Journal of Sustainable Energy, 37:7, 654-668, DOI: 10.1080/14786451.2017.1334654

To link to this article: https://doi.org/10.1080/14786451.2017.1334654

Published online: 05 Jun 2017.

INTERNATIONAL JOURNAL OF SUSTAINABLE ENERGY, 2018
VOL. 37, NO. 7, 654–668
https://doi.org/10.1080/14786451.2017.1334654

Taylor & Francis
Taylor & Francis Group

A framework for determining improved placement of current energy converters subject to environmental constraints

Kurt Nelson[a], Scott C. James [b], Jesse D. Roberts[c] and Craig Jones[a]

[a]Integral Consulting Inc., Santa Cruz, CA, USA; [b]Departments of Geosciences & Mechanical Engineering, Baylor University, Waco, TX, USA; [c]Sandia National Laboratories, Albuquerque, NM, USA

ABSTRACT

A modelling framework identifies deployment locations for current-energy-capture devices that maximise power output while minimising potential environmental impacts. The framework, based on the Environmental Fluid Dynamics Code, can incorporate site-specific environmental constraints. Over a 29-day period, energy outputs from three array layouts were estimated for: (1) the preliminary configuration (baseline), (2) an updated configuration that accounted for environmental constraints, (3) and an improved configuration subject to no environmental constraints. Of these layouts, array placement that did not consider environmental constraints extracted the most energy from flow (4.38 MW-hr/day), 19% higher than output from the baseline configuration (3.69 MW-hr/day). Array placement that considered environmental constraints removed 4.27 MW-hr/day of energy (16% more than baseline). This analysis framework accounts for bathymetry and flow-pattern variations that typical experimental studies cannot, demonstrating that it is a valuable tool for identifying improved array layouts for field deployments.

ARTICLE HISTORY
Received 19 September 2016
Accepted 22 January 2017

KEYWORDS
Marine renewable energy; current-energy conversion; modelling; array layout subject to environmental constraints

1. Introduction

Power generation with hydrokinetic current-energy converters (CECs), often in the form of underwater turbines, is receiving growing global interest. Because of ongoing research aimed to improve reasonable investment and maintenance costs, reliability, and environmental safety, the technology may soon contribute to national and global energy markets. In remote areas, small-scale CEC energy from river, tidal, or ocean currents can provide a local power supply. However, there is a clear interest in understanding the potential environmental effects of CEC operation in coastal embayments, estuaries, or rivers, or of the cumulative impacts of these devices on aquatic ecosystems over years or decades of operation (DOE 2009a, 2009b; Javaherchi 2010; Hasegawa et al. 2011; Kartezhnikova and Ravens 2014). In particular, there is an awareness that altered sediment dynamics, and changes to the benthic environment must be considered before deploying arrays of CECs (Amoudry et al. 2009; Neill et al. 2009; Robins, Neill, and Lewis 2014; Martin-Short et al. 2015; Thiébot, du Bois, and Guillou 2015). There is an urgent need for practical, accessible tools and peer-reviewed publications to help industry and regulators evaluate environmental impacts and mitigation measures, while establishing best siting and design practices (Inger et al. 2009).

This article describes a framework designed to maximise the power generation of tidal energy converters (TECs) while simultaneously minimising potential environmental effects in the form

CONTACT Kurt Nelson knelson@integral-corp.com; sc_james@baylor.edu

of disturbances to the local benthic environment. TECs are a subset of CECs that are specifically deployed in tidal channels. This framework was applied to a TEC array in Cobscook Bay, Maine. Cobscook Bay is the first deployment location of Ocean Renewable Power Company's (ORPC) TidGen® units. One unit was deployed, with four more units intended to follow. The developed framework uses the Sandia National Laboratories Environmental Fluid Dynamics Code (SNL-EFDC) hydrodynamic modelling platform (James et al. 2010, 2011). SNL-EFDC is suitable for modelling the regional and field scale hydrodynamic trends investigated in this work, but it parameterises turbulence and does not account for vertical fluid accelerations associated with nonhydrostatic pressure gradients. Existing computational fluid dynamics (CFD) models are capable of partially resolving turbulence and computing the nonhydrostatic pressure in turbine simulations (Kang et al. 2012; Sotiropoulos, Kang, and Yang 2012; Yang et al. 2015), but they are computationally expensive. Thus, SNL-EFDC was selected for this research. The developed framework can however be implemented within any CFD model if increased flow resolution is required.

It is important to note that this framework is not a rigorous optimisation methodology. Rather, it outlines an approach to place TECs within a designated site area such that they have improved power-production potential with commensurately decreased impact to the benthic environment through a reduction in bed shear stresses. If a rigorous approach to specifically optimising the array layout for maximum power generation is sought, several different approaches have been proposed and Vennell et al. (2015) provide a nice review. One of the first TEC optimisation studies used the Fluent modelling package to simulate changes in power output of a central TEC subject to specified array layouts in a simplified (flat-bottomed) system (Bai, Spence, and Dudziak 2009). Power output of the central TEC varied from −8% to +7% depending on the array layout and spacing. Lee et al. (2010) conducted a similar study (flat-bottomed) with STAR-CD to estimate turbine efficiencies subject to several specified lateral and longitudinal spacings. Gebreslassie, Tabor, and Belmont (2015) also studied the effects of turbine spacing (turbines in a row in a flat-bottomed system) on power generation using large eddy simulation in the open-source code, OpenFOAM. Both Vennell (2011) and Divett (2014) demonstrated how 'tuning' (varying the number and placement of TEC rows) impacted power generation in a flat-bottomed tidal channel. In the first published study where TECs were not restricted to an array layout in rows, Funke, Farrell, and Piggott (2014) allowed turbine locations to vary such that average turbine power was maximised. This study considered three idealised cases (channel flow, flow around a 90° bend, and channel flow around a circular island), as well as a flow through the Inner Sound of the Pentland Firth, yet all cases assumed flat bottoms to avoid complication of the analysis. Most recently, González-Gorbeña, Qassim, and Rosman (2016) used surrogate modelling to vary the placement of TECs in a flat-bottomed irregular channel where turbines were aligned in rows (either inline or staggered). While these studies provide the groundwork for array optimisation, to the authors' knowledge, we report the first array placement framework that uses natural flow conditions and site bathymetry.

SNL previously built a coarse-grid (100×100 m^2 cells), regional-scale hydrodynamic model (larger domain in Figure 1) that includes Cobscook Bay and all other landward embayments (O'Donncha, James, and Ragnoli 2017). Model results with and without a TEC array were compared to assess how the small, five-TEC array might alter the Cobscook Bay hydrodynamic environment. No significant changes in regional tidal range, flow rate, or broader flow patterns were identified. The coarse-grid size of the regional-scale model, however, is not sufficiently resolved to assess flow alterations in close proximity to the devices; the model has limited applicability for assessing local flow patterns and optimal device-placement locations. A refined-grid model was therefore created to meet the resolution demands of this optimisation framework.

The previously developed regional-scale model encompasses outer, central, and inner Cobscook Bay as shown in Figure 1 (Roberts and James 2012). The domain was gridded with 100×100-m^2 cells, with bottom elevations defined with interpolated bathymetric data obtained from the National Oceanographic and Atmospheric Administration National Geophysical Data Center. Circulation was driven in the model by water elevations specified at the inlet boundary on the east side of the

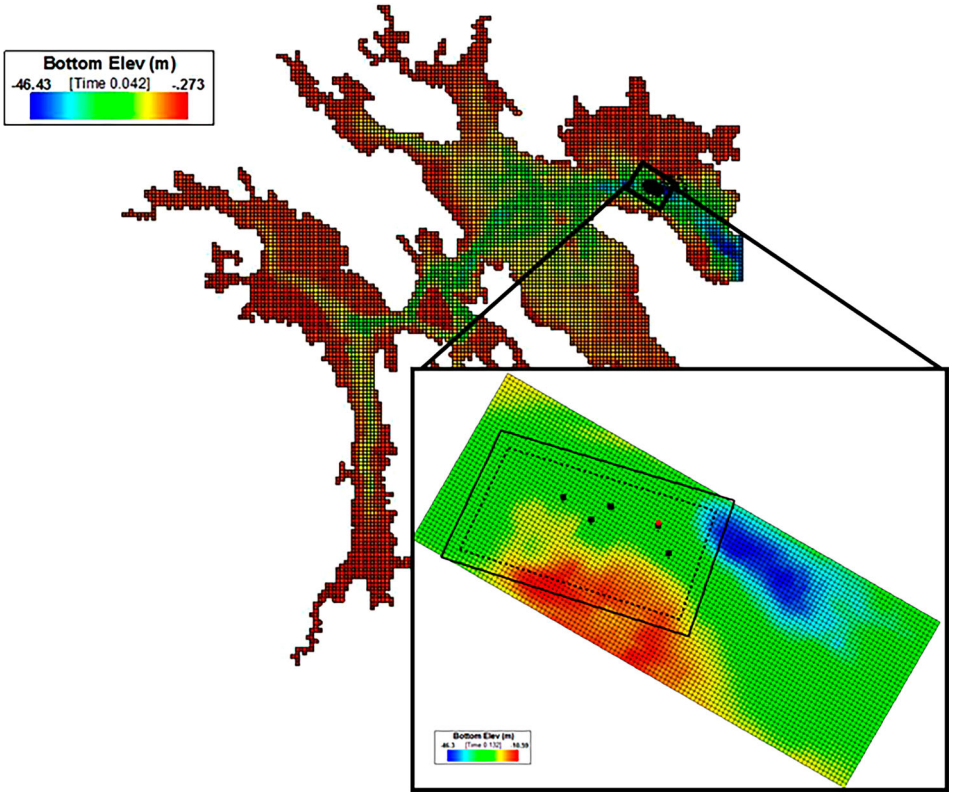

Figure 1. Regional-scale domain with an inset showing the refined-grid domain. Proposed locations of TEC devices (black squares) and ADCP deployment (red circle) are identified. The study region is outlined in the refined-grid domain with a solid black rectangle, and the placement footprint is outlined with a dashed black rectangle.

model domain (Figure 1). The specified water elevations were taken from a tidal station in Eastport, Maine, from 5 July to 2 August 2011 (NOAA 2014).

Modelled water levels taken from subsequent simulations were compared to measured water levels throughout the bay; the modelled values are typically within 14% of the observed values during tidal peaks, relative to mean lower low water (MLLW). For further validation, modelled and measured water velocities were also compared. ORPC measured velocities with a moored acoustic Doppler current profiler (ADCP) from 5 July through 2 August 2011, at UTM-NAD83 654,267-E, 4,974,792-N (red circle in callout of Figure 1). Depth-averaged velocity magnitudes computed by SNL-EFDC are generally close to the measured velocities, with the modelled results being on average 5% lower than the measured results. Our results are similar to those of Bao and Xue (2012) in that the model accurately reproduced the phase and trend of flows, but peak magnitudes were slightly underpredicted.

The regional-scale model of Cobscook Bay adequately simulated regional-scale circulation and reproduced available data sets for three water-level locations and ADCP-measured velocities. Upon comparing simulations with and without the proposed array of TECs, no significant changes were observed in tidal range, flow rate, or water velocity. Operations of this five-TEC array have little to no effect on regional aquatic habitat or circulation (Roberts and James 2012). However, the relatively large grid size of the regional-scale model (100×100 m^2) can only resolve flow patterns on the order of kilometres. The ORPC TidGen® units are approximately 30 m wide; so regional-scale grid cells are roughly 3.3 times the size of the TEC device. While this is sufficient for investigating large-scale environmental effects, near-field hydrodynamics important to fish swimming patterns and

local benthic habitat are not resolved. Therefore, a local, refined-grid model was developed using a resolution smaller than the individual turbines and their wakes. A brief preliminary effort of this sort by Roberts et al. (2014) introduced some of the concepts that are fully developed here.

2. Model setup

2.1. The EFDC model

The hydrodynamic portion of EFDC solves the hydrostatic, free-surface Reynolds-averaged Navier–Stokes (RANS) equations with Mellor–Yamada turbulence closure (Mellor and Yamada 1982) as modified by Galperin et al. (1988). This is similar to the model of Blumberg and Mellor (1987) except for the solution of the free surface, which is solved with a preconditioned conjugate gradient solver. As implemented here, EFDC uses a Cartesian grid with a sigma vertical coordinate system (Hamrick 2007a, 2007b) with each layer assigned a constant, equal fraction of the flow depth throughout the model domain. The thickness of each layer changes with the topology of the model domain and water depth. EFDC's time integration uses a second-order finite-difference scheme with a mode-splitting procedure to separate internal waves (baroclinic mode) from the external free-surface gravity wave (barotropic mode) for computational efficiency. EFDC has been extensively applied, validated, and documented at numerous sites worldwide, including estuaries, wetlands, lakes, rivers, and coastal environments (Ji, Morton, and Hamrick 2001; Tuckey et al. 2006; Ji 2008; Peng et al. 2011). The model has also been validated against analytical solutions, laboratory experiments, and real flow systems (James, Shrestha, and Roberts 2006; James, Janardhanam, and Hanson 2013).

2.2. Local domain size and parameters

The local model domain comprises 10×10-m^2 grid cells and encompasses the entire site footprint approved for ORPC. The local domain is 1120 m long, 430 m wide (4186 cells in the horizontal), and uses five vertical (sigma) layers. To simplify boundary specifications and best capture flow patterns, the domain was rotated 30°, approximately equal to the direction of net flow in the device-placement region. The inset in Figure 1 shows the refined model nested within the regional model, where the study region is outlined with a solid black rectangle. The region available for device placement, known as the placement footprint, is outlined with a dashed black rectangle. The potential placement footprint is 30.5 m (100 ft) within the border of the study area. The southeast (leftmost) boundary of the domain was extended past the relatively deep trench (~45 m deep) on the east side of the placement footprint to reduce numerical instabilities resulting from sharp bathymetry gradients.

2.3. Forcing conditions

The refined-grid model was driven by water levels and flow rates extracted from the regional-scale Cobscook Bay model (Roberts and James 2012; O'Donncha, James, and Ragnoli 2017). A time-variant water level was specified on the northwest face, and flow rates were specified on the southeast face. The two longer domain edges (northeast and southwest faces) were no-flux, slip wall conditions.

2.4. Hydrodynamic model calibration

When flow rates were transferred from the regional-scale Cobscook Bay model to the refined-grid domain, scaling was required. Flow rates were calculated within SNL-EFDC (Hamrick 2007a, 2007b) as a function of local, depth-averaged flow speed and water depth. Because of a factor of

10 refinement in grid cell size, bathymetric features were more accurately represented in the refined-grid domain. A combination of the approximate alignment of the local domain with the regional flow, specification of the northeast boundary as a uniform water elevation, and the more accurate depth representation led to discrepancies in calculated flow rates. The overall trends outputted from the regional-scale domain with respect to relative flow magnitude and direction were accurate, but the specified boundary flows required scaling to ensure a match between the regional model and the higher resolution of the refined-grid model.

ADCP data collected by ORPC were used to calibrate a flow-scaling factor. Flow rates directly extracted from the regional-scale domain were first used to drive the refined model. Velocity magnitudes from the refined-grid domain at the location of the ADCP were then compared to actual ADCP measurements. The modelled velocities were higher than the measured velocities; so a series of simulations were run at various fractions (0.55, 0.60, 0.65, 0.70, 0.75, 0.80, 0.85, and 0.90) of the output flow rates from the regional-scale model. All other parameters (e.g. outlet water levels) were held constant. Peak flood tides were often best matched by scaling the regional-scale flow predictions by a factor between 0.70 and 0.85, while ebb tides were best matched using a scaling factor between 0.55 and 0.65. To calibrate the refined-grid domain, the scaling factor that best fit each tidal peak was identified and applied to the specified-flow boundary. Simulated velocities from the calibrated refined-grid model are compared to ADCP measurements in Figure 2. The calibrated velocities closely match the ADCP measurements for the entire deployment/simulation period of 5 July through 2 August 2011.

Consistent with the regional model, the dimensionless Smagorinsky (1963) constant, which impacts the horizontal momentum transfer proportionally to the local horizontal strain rate, was set to 1, and the vertical eddy viscosity was set to 10^{-7} m^2/s. Bottom roughness was set to 2 cm

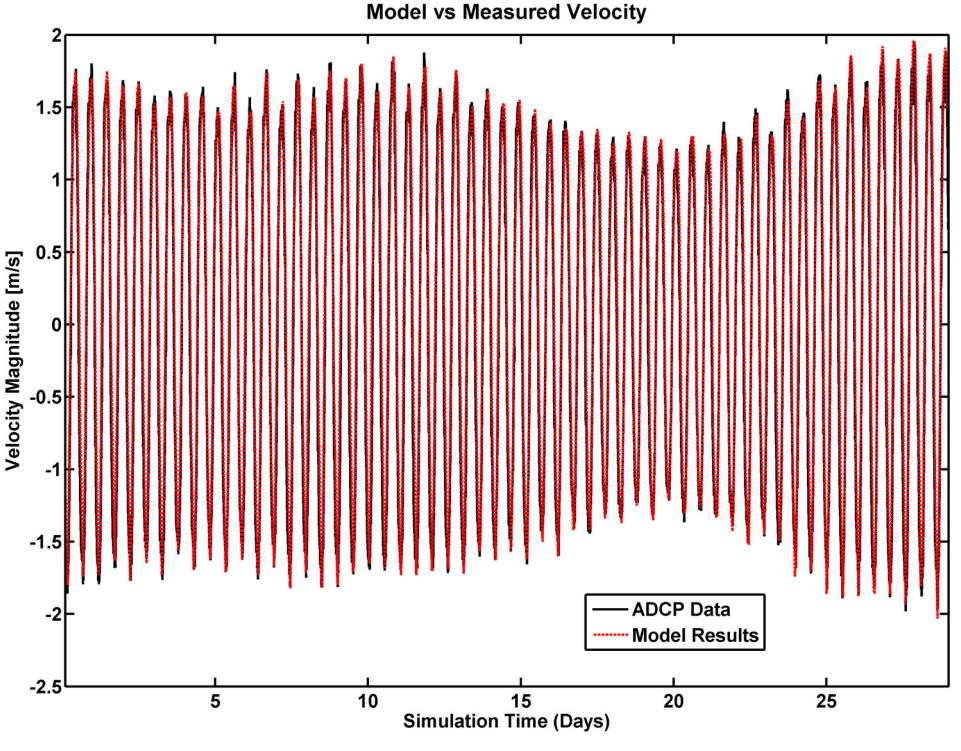

Figure 2. Comparison of velocities (m/s) between the measured ADCP data (black) and model-predicted values (red). Negative velocities indicate ebb tide.

everywhere. The model was spun up from rest for the two days preceding the commencement of ADCP data collection to specify a restart file with appropriate initial flows and water levels. The time step was set to 0.25 s. Wind waves were ignored.

2.5. Incorporation of TEC devices

The power generated by TEC turbines comes from energy removed from the flow passing through the swept area of the turbine blades. This behaviour is represented in SNL-EFDC using momentum sink and sources of turbulent kinetic energy and turbulent length scale at model cells containing turbines. Momentum extraction and wake generation and dissipation depend on both the properties of the turbines and the incident flow conditions. Power removed from flow by a turbine is given by (James et al. 2011)

$$P = \frac{1}{2} C_T \rho A_T U^3, \tag{1}$$

where C_T (–) is the thrust coefficient, ρ (kg/m^3) is the fluid density, A_T (m^2) is the cross-sectional flow-facing area of the TEC turbine, and U (m/s) is the incident velocity. Because the presence of the TEC alters the model-calculated U, the thrust coefficient in the preceding equation was modified as (Roc, Conley, and Greaves 2013)

$$C'_T = 4\frac{1 - \sqrt{1 - C_T}}{1 + \sqrt{1 - C_T}}. \tag{2}$$

Turbines were assumed to be aligned with the primary flow direction (although this may not always be true in a three-dimensional, bidirectional flow). Given this formulation and the turbine blade-swept area, the force, F, applied on the flow by the TEC device ($F = P/U$) was calculated. This force was decomposed into vector components based on the incident flow direction. Area-weighted forces were then applied to the flow at each vertical face of the model cell in which the TEC resided. If the TEC device occupied only a portion of a vertical (sigma) model layer, appropriate weighting was applied.

Corresponding changes to the turbulent kinetic energy and the turbulence length scale were implemented using the same physics that describe flow through a vegetative canopy (Katul et al. 2004), which has also been used in the wind-energy community (Réthoré, Sørensen, and Zahle 2009). Source and sink terms S_Q, S_k, and S_ℓ (specific to device type) represent the rate of momentum reduction, net change to turbulent kinetic energy, and the increase in turbulence length scale, respectively. In addition to effects from the TEC rotor, the effects of affiliated support structures were equivalently considered.

Momentum loss, S_Q (m/s^2), change in turbulent kinetic energy, S_k (m^2/s^3), and increase in turbulence length scale, S_ℓ (m^3/s^3) due to a TEC turbine were parameterised in the RANS and turbulence closure equations (Katul et al. 2004; Batten, Harrison, and Bahaj 2013):

$$S_Q = -\frac{1}{2} C_T A_d U^2, \tag{3}$$

$$S_k = \frac{1}{2} C_T A_d (\beta_p U^3 - \beta_d U k), \tag{4}$$

$$S_\ell = C_{\ell 4} S_k \ell, \tag{5}$$

where A_d (m^2/m^3) is the area density of a turbine within a cell, β_p (–) is an empirical coefficient indicating the fraction kinetic energy transferred into turbulence by the turbine (or support structure), β_d (–) is an empirical coefficient accounting for the fraction of turbulent kinetic energy, k (m^2/s^2), converted into turbine motion (or dissipated as heat by the support structure). ℓ (m) is the turbulence length scale computed as $k^{3/2}/\varepsilon$, where ε (m^2/s^3) is the turbulent kinetic energy dissipation rate, and

$C_{\ell 4}$ (−) is a closure constant. Calibrating SNL-EFDC-simulated wakes to available data collected from scaled three-bladed turbines in laboratory flumes (Myers and Bahaj 2009, 2010; Neary et al. 2012) yielded $\beta_p = 0.96$, $\beta_d = 1.38$, and $C_{\ell 4} = 3.87$ (James, Cardenas, and Hirlinger 2015). These values were calibrated to flume experiments and should be revisited when full-scale turbine wake data become available.

2.5.1. The TidGen® turbine

TidGen® cross-flow turbines are 30.28 m (100 ft) long and 4.3 m (14.1 ft) high, with blade bottoms 9 m (29.5 ft) from the sediment bed. The support structures are 3 m (9.8 ft) wide and extended from the sediment bed to a height of 11.2 m (36.7 ft). Figure 3 is a schematic representation of a TidGen® unit. Turbines were added to the refined-grid domain once the boundary-condition scaling was determined. Each device spanned roughly three cells. An conservative (large) thrust coefficient of 0.8 was specified; physical environmental changes are expected to increase as more energy is removed from the system. Different turbine properties can be implemented in future analyses as device-specific data become available.

2.5.2. Effects of turbines on flow

The model was run for the entire 29-day time period for which ADCP data were available with and without the preliminary ORPC-defined, five-turbine array layout. Momentum removed from the flow by the devices resulted in a velocity deficit in the wake of each turbine. Figure 4 shows representative velocity contours calculated during flood tide, where the turbine locations are indicated by black squares; the location of the ADCP is labelled with a red circle. Bathymetry influences flow direction and magnitude; velocities were general higher in shallower regions because of flow diversion. When peak flows occur and the greatest amount of water flows through the turbine blades and around the support structure, velocities are decreased within the TEC array.

The extent and recovery of the turbine wake was investigated by comparing model results with and without turbines. Initial results indicate that during both ebb and flood tides, the velocity deficit (difference between velocity with and without the turbines) reached its maximum roughly 15–25 m behind the devices. The magnitude of the deficit depended upon the incident flow velocity; stronger currents led to larger deficits. During peak flow events, the maximum velocity deficit was between 40% and 60%.

Flow that passes through the device loses momentum as kinetic energy from the flow is transferred to the rotational momentum of the blades, which are connected to an electricity generator. Downstream flow then increases as momentum diffuses back into the wake from adjacent fluid. Flow velocities typically recovered to 95% of their incident magnitude within 130 m. The extent of the wake depended upon the incident velocity, bathymetry, and the proximity of other devices.

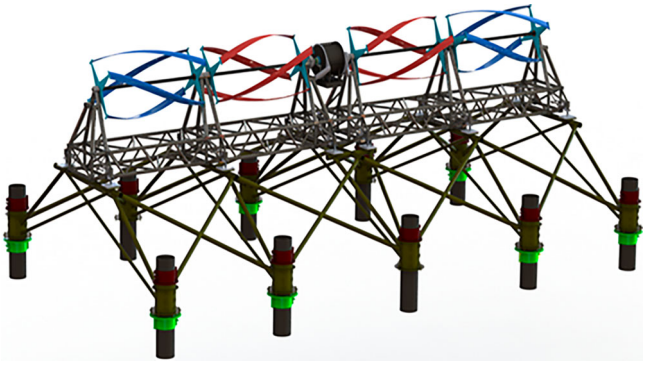

Figure 3. Schematic of the ORPC TidGen® turbine.

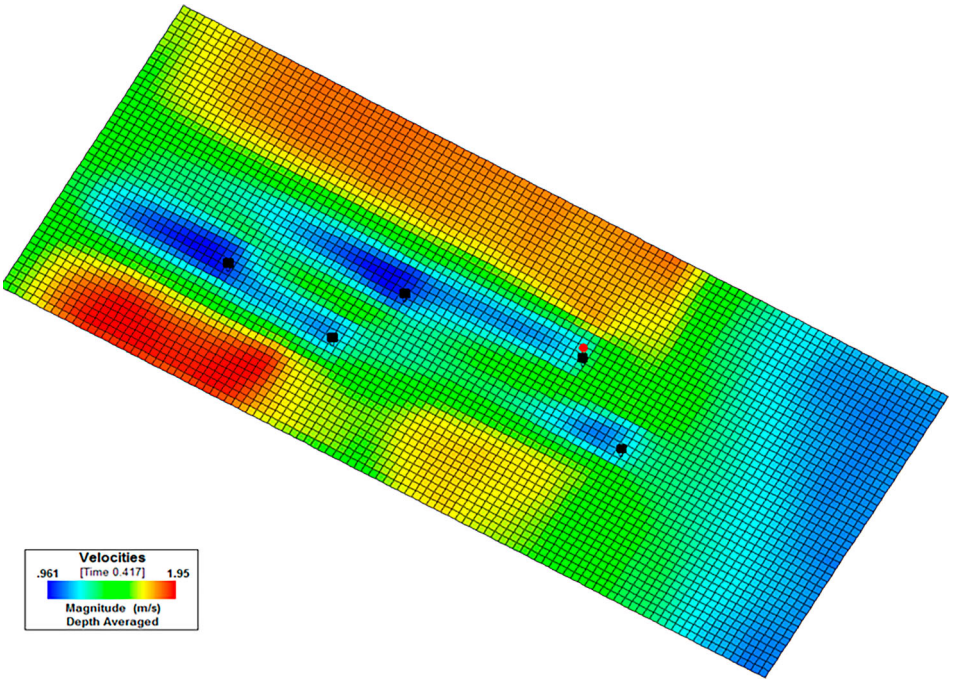

Figure 4. Contours of flow speed (m/s) during a typical flood tidal cycle. Wakes are seen behind the TEC devices. The centre locations of the devices are marked by a black square, and the ADCP location is marked by a red circle.

3. Placement framework and application

The proposed array configuration for the five-TEC array was only one possible selection among nearly an infinite number of possible layouts. As long as deployment locations fall within the placement footprint and are in a water depth greater than 23 m (75 ft) MLLW, the location can be considered for deployment. The depth restriction was provided by ORPC (as defined in the Federal Energy Regulatory Commission permit) and chosen to ensure sufficient clearance between the top of the devices and the water surface, allowing safe vessel passage.

3.1. Methodology for improved array configuration

To narrow down the near infinite number of possible array configurations within the permitted placement footprint, a methodology was developed to sequentially identify improved device-placement locations using SNL-EFDC. The procedure as applied to Cobscook Bay is:

(1) Assess the natural hydrodynamic patterns occurring within the placement footprint (no TEC devices).
(2) Identify the region within the footprint with the highest velocities at turbine depth, spanning the length (30 m) of the turbine. This region must be no less than 23 m (75 ft) below the MLLW.
(3) Add a TEC device in the high-velocity region identified in Step 2, and run simulations to reassess hydrodynamics in the placement footprint, given the TEC addition.
(4) Evaluate the hydrodynamic changes caused by the addition of the TEC turbine. Velocity and bed shear stress changes were examined by calculating percent velocity recovery and bed shear stress

differences. Percent velocity recovery is defined as:

$$R_{\%} = 100\frac{V_{\mathrm{TEC}}(i)}{V_{\mathrm{natural}}(i)}, \tag{6}$$

where $R_{\%}$ is the percent velocity recovery in cell i, $V_{\mathrm{TEC}}(i)$ is the velocity in cell i from a simulation with the TEC(s), and $V_{\mathrm{natural}}(i)$ is the velocity in cell i from a simulation without the TEC (s). Bed shear stress was calculated using the quadratic stress law:

$$\tau = \rho C_f v_{\mathrm{B}}^2, \tag{7}$$

where v_{B} (m/s) is the water velocity at the bed and C_f (–) is the bottom friction coefficient (Parker 2004):

$$C_f = \left[\frac{\kappa}{\ln(h/k_{\mathrm{s}})}\right]^2, \tag{8}$$

where κ is von Karman's constant (0.4) and $k_{\mathrm{s}} = 0.05$ (m) is the effective bed height roughness. Finally, the change in bed shear stress due to the presence of the device was calculated as:

$$\tau_{\mathrm{diff}} = \tau_{\mathrm{TEC}(i)} - \tau_{\mathrm{natural}}, \tag{9}$$

where τ_{diff} is the difference in shear stress between natural conditions (τ_{natural}) and with the addition of a TEC device ($\tau_{\mathrm{TEC}(i)}$).

(5) If pertinent, establish thresholds for $R_{\%}$ and τ_{diff} that meet local environmental standards. Check if $R_{\%(i)}$ and $\tau_{\mathrm{diff}(i)}$ are acceptable for all cells within the domain. If they are not acceptable, go back to Step 2 but choose the second-highest velocity location. To illustrate how these criteria operate within this analysis, a minimum threshold was set at $R_{\%(i)} \geq 70$ (i.e. depth-averaged velocities cannot drop below 70% of what they are without the presence of a turbine), and $\tau_{\mathrm{diff}} \leq 1$ Pa.

(6) Repeat Steps 2 through 6 for each additional turbine.

This methodology identifies regions where velocities are largest, thereby improving the power output of deployed TEC turbines. At the same time, environmental considerations are assessed to avoid array configurations that could notably effect local sediment dynamics and ecology. In the Cobscook Bay application of this methodology, arbitrary threshold values were assigned. However, site assessments by regulatory agencies or device manufacturers might better define acceptable, site-specific $R_{\%}$ and τ_{diff} values. Site assessments should consider local ecological systems and how changes in velocities and bed shear stress could potentially change their natural state. Sediment properties should also be considered. Knowing critical shear stresses in the vicinity of the turbines would provide insight into whether or not an increase or decrease in bed shear stress will increase or decrease sediment mobilisation and τ_{diff} limits could be defined accordingly.

For Cobscook Bay, velocity patterns were originally analysed over several tidal cycles. Multi-day simulations were computationally demanding and required more than 24 hours of computing time. The velocity contours showed spatial patterns during both ebb and flood tides that were similar between events. Flow patterns predicted during ebb or flood tides are self-similar; only the magnitude of the velocities of these events changed. To demonstrate this commonality, velocity magnitudes extracted during 10 peak tidal events (the five highest ebb and five highest flood tides from the 29-day simulation period) were averaged and compared to the velocity contours created by averaging velocities from two short simulations representative of typical maximum ebb and flood tides. The spatial velocity patterns predicted by simply forcing the model by representative maximum conditions closely matched those of the 10-peak average. The self-similarity allows this framework to be applied using hydrodynamic results modelled during a typical maximum ebb and flood tidal flow and not over the entire calibration period, thus significantly reducing computational demands.

The optimisation analysis was started by modelling the flow patterns during a typical maximum ebb and flood event (the same forcing conditions that were compared to the 10-peak average results) around the turbine that was actually deployed in Cobscook Bay. The predicted velocities extracted at roughly the depth of the turbine (sigma layer three) were averaged to identify high-velocity regions within the placement footprint. Sigma layer three ebb- and flood-averaged velocity contours are presented in the left panel of Figure 5, where the placement footprint is outlined by a white rectangle and the location of the deployed turbine is indicated with three adjacent grey cells. Because the velocity contours plotted are the result of averaging an ebb and flood event, the wake created by the turbine is depicted on both upstream and downstream sides of the device.

In the left panel of Figure 5, cells with depths less than 23 m (75 ft) were blacked out. This depth threshold was applied to limit potential placement regions to those that are sufficiently deep to avoid risks to shipping lanes. Next, the three adjacent cells with the highest average velocity were located (circled in grey in the left panel of Figure 5). The $R_{\%}$ and τ_{diff} in each cell were then calculated and checked to ensure $R_{\%}$ was above 70% and τ_{diff} was below 1 Pa throughout the domain (currently specified constraints). Contour plots of $R_{\%}$ and τ_{diff} are presented in the middle and right panel of Figure 5. Because the threshold criteria were met for both $R_{\%}$ and τ_{diff}, a second TEC was added within the domain to the domain. This process was repeated until deployment locations for all five turbines had been identified (Figure 6).

When locating the best placement location for the fourth and fifth TEC devices, several simulations were run before identifying a deployment location that was in a region of high flow and did not exceed the threshold criteria for $R_{\%}$ or τ_{diff}. Because the threshold criteria were chosen to illustrate their functionality within the analysis, potential power gain resulting from no environmental constraints was also modelled. The framework was applied a second time, ignoring $R_{\%}$ and τ_{diff} criteria. The three five-TEC arrays analysed during the present study are shown in Figure 7, including the preliminary ORPC-defined configuration, the configuration that *accounted for* environmental constraints, and the configuration that *did not consider* environmental constraints. Each panel in Figure 7 is contoured with $R_{\%}$ calculated from sigma-layer-three velocities.

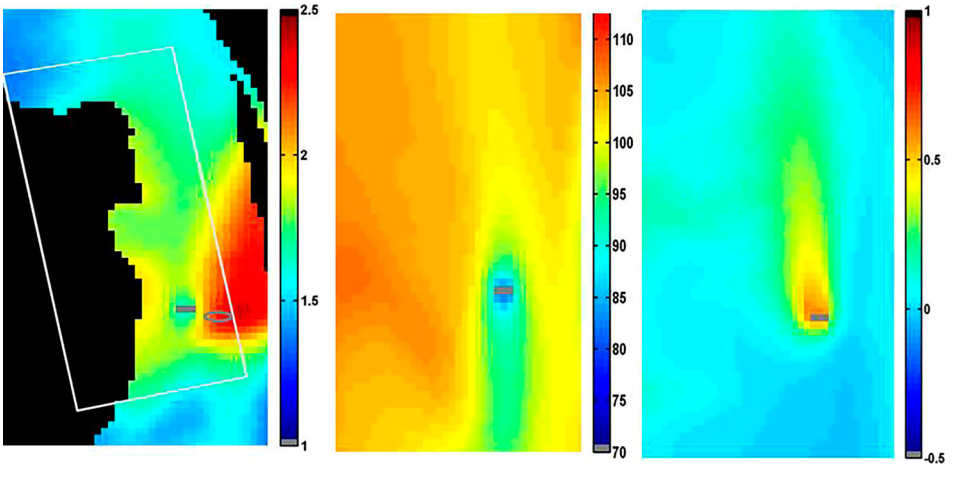

Figure 5. Averaged ebb and flood velocity contours (m/s) (left panel), $R_{\%}$ (unitless) (centre panel), and τ_{diff} (Pa) predicted by simulating one TEC device (right panel). The placement footprint is outlined by a white rectangle in the left panel, and the improved deployment location of the next TEC device is marked by the grey oval. Cells with depths less than 23 m are blacked out.

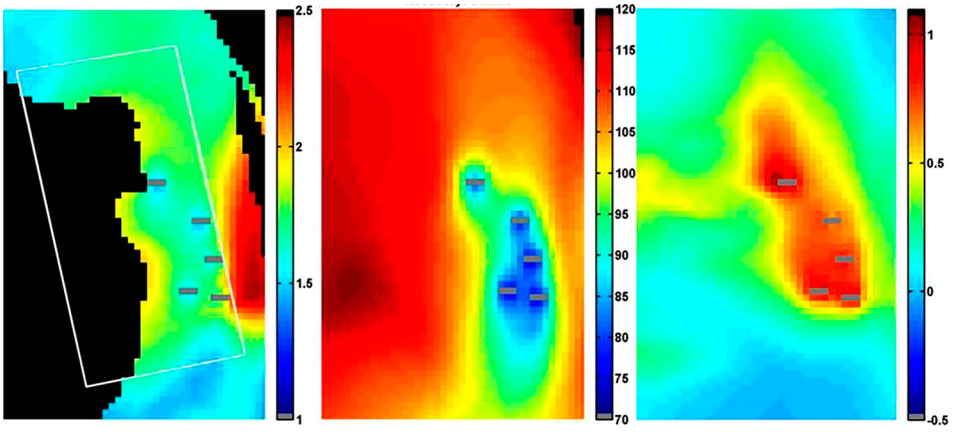

Figure 6. Averaged ebb and flood velocity contours (m/s) (left panel), $R_{\%}$ (unitless) (centre panel), and τ_{diff} (Pa) predicted by simulating five-TEC devices (right panel).

3.2. Array performance

Changes in placement locations of the TidGen® units altered the power removed from the water by the array over the 29-day simulation period. Of the three configurations analysed, the array placed *without* environmental constraints produced the largest amount of energy, at 4.38 MW-hr/day. This output was roughly 19% higher than the output from the preliminary ORPC array configuration (3.67 MW-hr/day). For the array *with* environmental constraints, 4.27 MW-hr/day was removed (16% increase from the preliminary array).

The performance of a TEC is directly related to the fluid momentum normal to the device blades. Accordingly, wake recovery is highly important to device performance. When assessing the optimal placement of a TEC array in a real-world application, where bathymetry and flow patterns significantly change both spatially and temporally, generalising wake recovery and the appropriate spacing between devices is challenging. Wake recovery depends on several factors, including water depth, turbulence (Blackmore, Batten, and Bahaj 2014), and local flow patterns. Idealised flume experiments often do not account for these factors; however, this framework does.

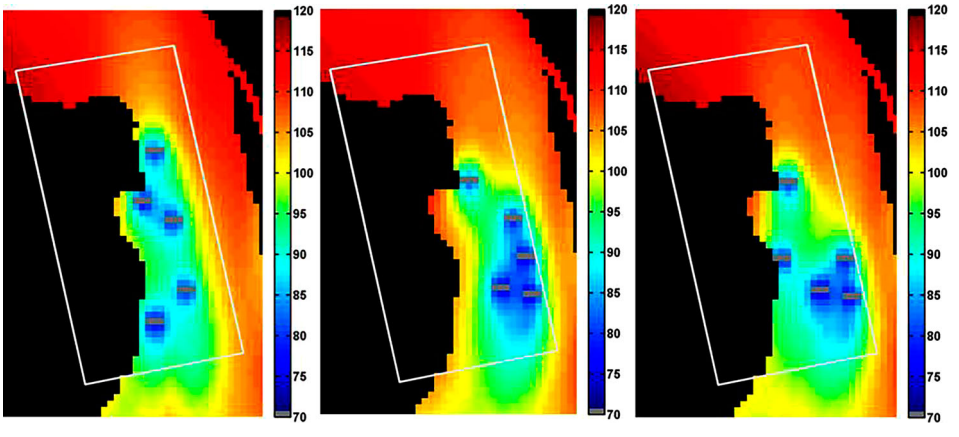

Figure 7. The 3 five-TEC arrays investigated: preliminary ORPC-defined array (left panel), environmentally constrained array layout (centre panel), and unconstrained array layout (right panel). All three plots are colour-contoured with $R_{\%}$ (unitless).

3.3. Environmental considerations

This framework facilitates straightforward implementation of environmental constraints. The analysis considered arbitrary changes in flow and seabed shear stress where $R_{\%}$ and τ_{diff} were defined as the primary constraints. However, this framework is flexible such that these constraints can be easily modified to meet site requirements and needs. As studies progress at CEC deployment sites, environmental constraints for a given site should be developed collaboratively with local stakeholders, other scientists (i.e. biologists, ecologists, and geologists), device and project developers, and the modelling team to best address site-specific concerns. For example, if an ecologist determines that the benthic activity will change near a proposed deployment location if shear stresses increase by 25%, a percent change constraint could be defined for bed shear stress and incorporated into the analysis instead of, or in addition to, τ_{diff}. Although the limited domain of the local-scale model facilitates trend investigations only near the array, once the array has been optimally configured, TEC locations can be included in a regional-scale model to evaluate environmental impacts such as changes to tidal range and flushing.

4. Conclusions

A framework was created to determine improved deployment locations for TECs by maximising power output while minimising potential environmental impacts induced by deployed devices. The framework is flexible and can be adjusted to incorporate site-specific environmental constraints. To demonstrate the framework's applicability, a five-TEC array in Cobscook Bay, Maine, was investigated.

A coarse-grid, regional-scale model of Cobscook Bay previously demonstrated that the operation of five ORPC tidal turbines would not cause significant changes in regional tidal range, flow rate, or broader flow patterns. While the model was sufficient for investigating large-scale environmental effects, near-field hydrodynamics were not resolved. Therefore, a refined-grid model with a resolution smaller than the individual turbines was created and implemented in this framework.

The energy output of three array layouts was estimated over a 29-day period. This included the preliminary ORPC-defined configuration (baseline), an improved configuration that *accounted for* arbitrary environmental constraints as well as an improved configuration that *did not consider* environmental constraints. Of the three layouts analysed, the array layout that *did not consider* environmental constraints removed the largest amount of energy from the water, at 4.38 MW-hr/day. This output was roughly 19% higher than the output from the preliminary ORPC array configuration (3.68 MW-hr/day). The optimally placed array that *accounted for* environmental constraints removed 4.27 MW-hr/day of energy (16% increase from the preliminary array).

When assessing potential placements of TECs in an array in a real-world application, where bathymetry and flow patterns change both spatially and temporally, generalising wake recovery and the appropriate spacing between devices is challenging. The difficulties arise due to spatial and temporal variations in turbulence and flow, which both affect wake recovery. The framework presented accounts for these variations, making it a valuable tool for improving array layouts subject to environmental constraints.

Acknowledgements

EFDC Explorer (Craig 2011) was used to visualise many of the model results.

Disclosure statement

No potential conflict of interest was reported by the authors.

Funding

This research was made possible by support from the Department of Energy's Energy Efficiency and Renewable Energy (EERE) Wind and Water Power Program. Sandia National Laboratories is a multi-mission laboratory managed and operated by Sandia Corporation, a wholly owned subsidiary of Lockheed Martin Corporation, for the U.S. Department of Energy's National Nuclear Security Administration under contract DE-AC04-94AL85000.

ORCID

Scott C. James http://orcid.org/0000-0001-7955-0491

References

Amoudry, L., P. S. Bell, K. S. Black, R. W. Gatliff, R. Helsby, A. J. Souza, P. D. Thorne, and J. Wolf. 2009. *A Scoping Study on: Research Into Changes in Sediment Dynamics Linked to Marine Renewable Energy Installations*. Edinburgh: British Geological Survey.

Bai, L., R. R. G. Spence, and G. Dudziak. 2009. "Investigation of the Influence of Array Arrangement and Spacing on Tidal Energy Converter (TEC) Performance Using a 3-Dimensional CFD Model." 8th European Wave and Tidal Energy, 654–660, Uppsala, Sweden.

Bao, M., and H. Xue. 2012. "Evaluating the Tidal Stream Power and Impacts of Energy Extraction on Hydrodynamics in Cobscook and Passamaquoddy Bays." Paper presented at the AGU Ocean Sciences, Salt Lake City, UT, February 20–24.

Batten, W. M. J., M. E. Harrison, and A. S. Bahaj. 2013. "Accuracy of the Actuator Disc-RANS Approach for Predicting the Performance and Wake of Tidal Turbines." *Philosophical Transactions of the Royal Society A: Mathematical, Physical and Engineering Sciences* 371: 20120293. doi:10.1098/rsta.2012.0293.

Blackmore, T., W. M. J. Batten, and A. S. Bahaj. 2014. "Influence of Turbulence on the Wake of a Marine Current Turbine Simulator." *Proceedings of the Royal Society A: Mathematical, Physical and Engineering Sciences* 470: 20140331. doi:10.1098/rspa.2014.0331.

Blumberg, A. F., and G. L. Mellor. 1987. "A Description of a Three-Dimensional Coastal Ocean Circulation Model." In *Three Dimensional Coastal Ocean Models Conference*, edited by Norman S. Heaps, 1–16. Washington, DC: American Geophysical Union.

Craig, P. M. 2011. *User's Manual for EFDC_Explorer: A Pre/Post Processor for the Environmental Fluid Dynamics Code*. EFDC_Explorer. Knoxville: Dynamic Solutions International.

Divett, T. A. 2014. *Optimising Design of Large Tidal Energy Arrays in Channels: Layout and Turbine Tuning for Maximum Power Capture Using Large Eddy Simulations with Adaptive Mesh*. Dunedin, New Zealand: University of Otago.

DOE. 2009a. *Potential Environmental Effects of Marine and Hydrokinetic Energy Technologies*. Washington, DC: Department of Energy.

DOE. 2009b. *Report to Congress on the Potential Environmental Effects of Marine and Hydrokinetic Energy Technologies*. GO-102009-2955. Washington, DC: Department of Energy.

Funke, S. W., P. E. Farrell, and M. D. Piggott. 2014. "Tidal Turbine Array Optimisation Using the Adjoint Approach." *Renewable Energy* 63: 658–673. doi:10.1016/j.renene.2013.09.031.

Galperin, B., L. H. Kantha, S. Hassid, and A. Rosati. 1988. "A Quasi-Equilibrium Turbulent Energy Model for Geophysical Flows." *Journal of the Atmospheric Sciences* 45 (1): 55–62. doi:10.1175/1520-0469(1988)045.

Gebreslassie, M. G., G. R. Tabor, and M. R. Belmont. 2015. "Investigation of the Performance of a Staggered Configuration of Tidal Turbines Using CFD." *Renewable Energy* 80: 690–698. doi:10.1016/j.renene.2015.03.001.

González-Gorbeña, E., R. Y. Qassim, and P. C. C. Rosman. 2016. "Optimisation of Hydrokinetic Turbine Array Layouts via Surrogate Modelling." *Renewable Energy* 93: 45–57. doi:10.1016/j.renene.2016.02.045.

Hamrick, J. M. 2007a. *The Environmental Fluid Dynamics Code: Theory and Computation*. EFDC Theory and Computation: Version 1.01. Fairfax, VA: US EPA.

Hamrick, J. M. 2007b. *The Environmental Fluid Dynamics Code: User Manual*. EFDC User Manual: Version 1.01. Fairfax, VA: US EPA.

Hasegawa, D., J. Sheng, D. A. Greenberg, and K. R. Thompson. 2011. "Far-field Effects of Tidal Energy Extraction in the Minas Passage on Tidal Circulation in the Bay of Fundy and Gulf of Maine Using a Nested-Grid Coastal Circulation Model." *Ocean Dynamics* 61 (11): 1845–1868. doi:10.1007/s10236-011-0481-9.

Inger, R., M. J. Attrill, S. Bearhop, A. C. Broderick, W. J. Grecian, D. J. Hodgson, C. Mills, *et al.* 2009. "Marine Renewable Energy: Potential Benefits to Biodiversity? An Urgent Call for Research." *Journal of Applied Ecology* 46: 1145–1153. doi:10.1111/j.1365-2664.2009.01697.x.

James, S. C., J. Barco, E. Johnson, J. D. Roberts, and S. Lefantzi. 2011. "Verifying Marine-Hydro-Kinetic Energy Generation Simulations Using SNL-EFDC." IEEE OCEANS 2011 conference, 1–9, Kona, Hawai'i.

James, S., M. Cardenas, and C. Hirlinger. 2015. "Validating and Applying SNL-EFDC to Current Energy Capture Devices Simulation." World environmental and water resources congress 2015, 1368–77, American Society of Civil Engineers.
James, S. C., V. Janardhanam, and D. T. Hanson. 2013. "Simulating pH Effects in an Algal-Growth Hydrodynamics Model." *Journal of Phycology* 49 (3): 608–615. doi:10.1111/jpy.12071.
James, S. C., E. Seetho, C. Jones, and J. Roberts. 2010. "Simulating Environmental Changes due to Marine Hydrokinetic Energy Installations." IEEE OCEANS 2010 conference, 1–10, Seattle, Washington.
James, S. C., P. L. Shrestha, and J. D. Roberts. 2006. "Modeling Noncohesive Sediment Transport Using Multiple Sediment Size Classes." *Journal of Coastal Research* 22 (5): 1125–1132. doi:10.2112/05-0497.1.
Javaherchi, A. T. 2010. *Numerical Modeling of Tidal Turbines: Methodology Development and Potential Physical Environmental Effects*. Seattle, WA: University of Washington.
Ji, Z.-G. 2008. *Hydrodynamics and Water Quality: Modeling Rivers, Lakes, and Estuaries*. Hoboken, NJ: John Wiley.
Ji, Z. G., M. R. Morton, and J. M. Hamrick. 2001. "Wetting and Drying Simulation of Estuarine Processes." *Estuarine, Coastal and Shelf Science* 53 (5): 683–700. doi:10.1006/ecss.2001.0818.
Kang, S., I. Borazjani, J. A. Colby, and F. Sotiropoulos. 2012. "Numerical Simulation of 3D Flow Past a Real-Life Marine Hydrokinetic Turbine." *Advances in Water Resources* 39 (0): 33–43. doi:10.1016/j.advwatres.2011.12.012.
Kartezhnikova, M. E., and T. M. Ravens. 2014. "Hydraulic Impacts of Hydrokinetic Devices." *Renewable Energy* 66: 425–432. doi:10.1016/j.renene.2013.12.034.
Katul, G. G., L. Mahrt, D. Poggi, and C. Sanz. 2004. "One- and two-Equation Models for Canopy Turbulence." *Boundary-Layer Meteorology* 113 (1): 81–109. doi:10.1023/B:BOUN.0000037333.48760.e5.
Lee, S. H., S. H. Lee, K. Jang, J. Lee, and N. Hur. 2010. "A Numerical Study for the Optimal Arrangement of Ocean Current Turbine Generators in the Ocean Current Power Parks." *Current Applied Physics* 10 (2): S137–S141. doi:10.1016/j.cap.2009.11.018.
Martin-Short, R., J. Hill, S. C. Kramer, A. Avdis, P. A. Allison, and M. D. Piggott. 2015. "Tidal Resource Extraction in the Pentland Firth, UK: Potential Impacts on Flow Regime and Sediment Transport in the Inner Sound of Stroma." *Renewable Energy* 76: 596–607. doi:10.1016/j.renene.2014.11.079.
Mellor, G. L., and T. Yamada. 1982. "Development of a Turbulence Closure Model for Geophysical Fluid Problems." *Reviews of Geophysics* 20 (4): 851–875.
Myers, L., and A. S. Bahaj. 2009. "Near Wake Properties of Horizontal Axis Marine Current Turbines." Proceedings of the 8th European wave and tidal energy conference, 558–65, Uppsala, Sweden.
Myers, L. E., and A. S. Bahaj. 2010. "Experimental Analysis of the Flow Field Around Horizontal Axis Tidal Turbines by Use of Scale Mesh Disk Rotor Simulators." *Ocean Engineering* 37: 218–227. doi:10.1016/j.oceaneng.2009.11.0044.
Neary, V. S., B. Gunawan, C. Hill, and L. P. Chamorro. 2012. *Wake Flow Recovery Downstream of a 1:10 Scale Axial Flow Hydrokinetic Turbine Measured with Pulse-Coherent Acoustic Doppler Profiler (PC-ADP)*. ORNL/TML-2012. Oak Ridge, TN: Oak Ridge National Laboratory.
Neill, S. P., E. J. Litt, S. J. Couch, and A. G. Davies. 2009. "The Impact of Tidal Stream Turbines on Large-Scale Sediment Dynamics." *Renewable Energy* 34 (12): 2803–2812. doi:10.1016/j.renene.2009.06.015.
NOAA. 2014. "Water levels at Eastport, ME - Station ID: 841014." Accessed June 30. http://tidesandcurrents.noaa.gov/stationhome.html?id=8410140.
O'Donncha, F., S. C. James, and E. Ragnoli. 2017. "Modelling Study of the Effects of Suspended Aquaculture Installations on Tidal Stream Generation in Cobscook Bay." *Renewable Energy* 102 (Part A): 65–76. doi:10.1016/j.renene.2016.10.024.
Parker, G. 2004. "1D Sediment Transport Morphodynamics, with Applications to Rivers and Turbidity Currents." E-book.
Peng, S., G. Y. Z. Fu, X. H. Zhao, and B. C. Moore. 2011. "Integration of Environmental Fluid Dynamics Code (EFDC) Model with Geographical Information System (GIS) Platform and Its Applications." *Journal of Environmental Informatics* 17 (2): 75–82. doi:10.3808/jei.201100189.
Réthoré, P.-E., N. N. Sørensen, and F. Zahle. 2009. "Study of the Atmospheric Wake Turbulence of a CFD Actuator Disc Model." European Wind Energy Convention, 1–9, Marseille, France.
Roberts, J. D., and S. C. James. 2012. *SNL-EFDC Model Application to Cobscook Bay, ME*. Albuquerque, NM: Sandia National Laboratories.
Roberts, J. D., K. Nelson, C. A. Jones, and S. C. James. 2014. "A framework for optimizing the placement of current energy converters." In 2nd Marine Energy Technology Symposium, edited by METS, 9. Seattle, WA: METS.
Robins, P. E., S. P. Neill, and M. J. Lewis. 2014. "Impact of Tidal-Stream Arrays in Relation to the Natural Variability of Sedimentary Processes." *Renewable Energy* 72: 311–321. doi:10.1016/j.renene.2014.07.031.
Roc, T., D. C. Conley, and D. Greaves. 2013. "Methodology for Tidal Turbine Representation in Ocean Circulation Model." *Renewable Energy* 51: 448–464. doi:10.1016/j.renene.2012.09.039.
Smagorinsky, J. 1963. "General Circulation Experiments with Primitive Equations 1: The Basic Experiment." *Monthly Weather Review* 91 (3): 99–164. doi:10.1175/1520-0493(1963)091.

Sotiropoulos, F., S. Kang, and X. Yang. 2012. "Large-eddy Simulation of Turbulent Flow Past Hydrokinetic Turbine Arrays in Natural Waterways." American Geophysical Union Fall Meeting, San Francisco, CA.

Thiébot, J., P. B. du Bois, and S. Guillou. 2015. "Numerical Modeling of the Effect of Tidal Stream Turbines on the Hydrodynamics and the Sediment Transport–Application to the Alderney Race (Raz Blanchard), France." *Renewable Energy* 75: 356–365. doi:10.1016/j.renene.2014.10.021.

Tuckey, B. J., M. T. Gibbs, B. R. Knight, and P. A. Gillespie. 2006. "Tidal Circulation in Tasman and Golden Bays: Implications for River Plume Behaviour." *New Zealand Journal of Marine and Freshwater Research* 40: 305–324.

Vennell, R. 2011. "Tuning Tidal Turbines In-concert to Maximise Farm Efficiency." *Journal of Fluid Mechanics* 671: 587–604. doi:10.1017/S0022112010006191.

Vennell, R., S. W. Funke, S. Draper, C. Stevens, and T. Divett. 2015. "Designing Large Arrays of Tidal Turbines: A Synthesis and Review." *Renewable and Sustainable Energy Reviews* 41: 454–472. doi:10.1016/j.rser.2014.08.022.

Yang, X., A. Khosronejad, S. Chawdhary, A. Calderer, D. Angelidis, L. Shen, and F. Sotiropoulos. 2015. "Simulation-Based Approach for Site-Specific Optimization of Marine and Hydrokinetic Energy Conversion Systems." In 36th IAHR World Congress, 1–4. The Hague, The Netherlands: Spain Water and IWHR.